Clinical Cancer Research

Tumor-Derived CCL2 Mediates Resistance to Radiotherapy in Pancreatic Ductal Adenocarcinoma

Anusha Kalbasi[1,2], Chad Komar[1,3], Graham M. Tooker[1,3], Mingen Liu[1,3], Jae W. Lee[1,3], Whitney L. Gladney[1,3], Edgar Ben-Josef[1,2], and Gregory L. Beatty[1,3]

Abstract

Purpose: Local tumor growth is a major cause of morbidity and mortality in nearly 30% of patients with pancreatic ductal adenocarcinoma (PDAC). Radiotherapy is commonly used for local disease control in PDAC, but its efficacy is limited. We studied the impact of selectively intervening on radiotherapy-induced inflammation as an approach to overcome resistance to radiotherapy in PDAC.

Experimental Design: PDAC cell lines derived from primary pancreatic tumors arising spontaneously in *Kras*$^{LSL\text{-}G12D/+}$; *Trp53*$^{LSL\text{-}R172H/+}$;*Pdx-1 Cre* mice were implanted into syngeneic mice and tumors were focally irradiated using the Small Animal Radiation Research Platform (SARRP). We determined the impact of depleting T cells and Ly6C$^+$ monocytes as well as inhibiting the chemokine CCL2 on radiotherapy efficacy. Tumors were analyzed by flow cytometry and IHC to detect changes in leukocyte infiltration, tumor viability, and vascularity. Assays were performed on tumor tissues to detect cytokines and gene expression.

Results: Ablative radiotherapy alone had minimal impact on PDAC growth but led to a significant increase in CCL2 production by tumor cells and recruitment of Ly6C$^+$CCR2$^+$ monocytes. A neutralizing anti-CCL2 antibody selectively inhibited radiotherapy-dependent recruitment of monocytes/macrophages and delayed tumor growth but only in combination with radiotherapy ($P < 0.001$). This antitumor effect was associated with decreased tumor proliferation and vascularity. Genetic deletion of CCL2 in PDAC cells also improved radiotherapy efficacy.

Conclusions: PDAC responds to radiotherapy by producing CCL2, which recruits Ly6C$^+$CCR2$^+$ monocytes to support tumor proliferation and neovascularization after radiotherapy. Disrupting the CCL2–CCR2 axis in combination with radiotherapy holds promise for improving radiotherapy efficacy in PDAC. *Clin Cancer Res; 23(1); 137–48.* ©*2016 AACR.*

Introduction

Clinical outcomes in pancreatic ductal adenocarcinoma (PDAC) are poor with a 5-year overall survival of only 7% (1, 2). Although metastasis is the most common cause of mortality, 30% of patients will succumb to disease due to complications of local tumor growth (3). In addition to its effect on mortality, local tumor growth can also cause significant morbidity including obstructive biliary sepsis, duodenal obstruction, and intractable pain related to celiac plexus involvement (4–6).

Approximately 25% of patients with PDAC will present with localized but unresectable disease (7); for these patients, radiotherapy is a major treatment modality for local control. However, local progression despite radiotherapy is common (8–10). Recently, stereotactic ablative body radiotherapy (SBRT or SABR) has garnered significant attention as a means to deliver a higher biologically effective radiation dose (11–16). Ablative radiotherapy has also been found to alter the immune response to cancer (17). In particular, for immunologically sensitive models of cancer, ablative radiotherapy can increase T-cell infiltration leading to durable remissions, as shown in a subcutaneous murine model of colon cancer (18). However, the impact of ablative radiotherapy on the immune microenvironment of immunologically resistant tumors, such as PDAC, remains ill-defined.

In PDAC, the tumor microenvironment is characterized by poor infiltration of effector T cells and a predominance of innate inflammatory cells, including macrophages (19, 20). This microenvironment is profoundly immunosuppressive and establishes a site of T-cell immune privilege (21). In addition, the microenvironment that surrounds PDAC is supportive of cancer growth, invasion, and metastasis (22, 23). However, the immune reaction to PDAC is inherently pliable such that myeloid cells responding to PDAC can also be induced with antitumor properties capable of enhancing the efficacy of standard cytotoxic therapies (19, 24).

[1]Abramson Cancer Center, University of Pennsylvania, Philadelphia, Pennsylvania. [2]Department of Radiation Oncology, Perelman School of Medicine, University of Pennsylvania, Philadelphia, Pennsylvania. [3]Division of Hematology-Oncology, Department of Medicine, Perelman School of Medicine, University of Pennsylvania, Philadelphia, Pennsylvania

Note: Supplementary data for this article are available at Clinical Cancer Research Online (http://clincancerres.aacrjournals.org/).

Corresponding Author: Gregory L. Beatty, University of Pennsylvania, Smilow Center for Translational Research, 8-112, 3400 Civic Center Blvd. Building 421, Philadelphia, PA 19104-5156. Phone: 215-746-7764; Fax: 215-573-8590; E-mail: gregory.beatty@uphs.upenn.edu

doi: 10.1158/1078-0432.CCR-16-0870

Translational Relevance

Pancreatic ductal adenocarcinoma (PDAC) has demonstrated substantial resistance to radiotherapy. Here, we report that PDAC responds to radiotherapy by releasing inflammatory molecules, including the chemokine CCL2. By recruiting inflammatory monocytes/macrophages to the tumor microenvironment to promote tumor proliferation and vascularization, tumor-derived CCL2 inhibited the efficacy of ablative radiotherapy in a mouse model of PDAC. In contrast, selective blockade of CCL2 using neutralizing antibodies blocked monocyte/macrophage recruitment to tumors and, in combination with radiotherapy, produced antitumor activity with enhanced survival. As primary tumor growth in PDAC is responsible for up to 30% of patient mortality, our findings highlight a potential role for targeting the inflammatory response to radiotherapy for improving local control and patient outcomes.

In this study, we examined the effect of ablative radiotherapy on the immune response to PDAC. Unlike immunologically sensitive tumors, radiotherapy did not induce T-cell infiltration into tumor tissue. In contrast, PDAC cells responded to radiotherapy by releasing inflammatory cytokines and chemokines including CCL2. Tumor-derived CCL2 induced an increase in inflammatory monocytes and macrophages within the tumor microenvironment and inhibited antitumor activity mediated by radiotherapy. In contrast, neutralization of CCL2 blocked inflammatory monocyte recruitment to tumors and resulted in improved tumor control when administered in combination with radiotherapy.

Materials and Methods

Animals

C57BL/6 mice were purchased from The Jackson Laboratories. Animal protocols were reviewed and approved by the Institute of Animal Care and Use Committee of the University of Pennsylvania (Philadelphia, PA).

Cell lines

Mouse pancreatic cancer cell lines were derived from spontaneously arising tumors in *Kras*$^{LSL\text{-}G12D/+}$, *Trp53*$^{LSL\text{-}R172H/+}$, *Pdx1-Cre* (KPC) mice as described previously (24, 25). Cell lines were authenticated on the basis of histologic analysis of the implanted cell line in comparison with the primary tumor from which the cell line was derived as described previously (24). Cell lines were tested for mycoplasma contamination, cultured at 37°C in DMEM supplemented with 10% FCS, 83 μg/mL gentamicin, and 1% L-glutamine, and used in experiments between 6 and 8 passages.

Animal experiments

PDAC cell lines were implanted subcutaneously at 4–5 × 10^5 cells into syngeneic C57BL/6 mice. For orthotopic implantation of tumor cells, syngeneic C57BL/6 mice were first anesthetized and the abdomen prepared in a sterile fashion. A small (5–10 mm) incision was made over the left upper quadrant of the abdomen, and the peritoneal cavity was exposed. The pancreas was then located and exteriorized onto a sterile field. PDAC cell lines (5 × 10^5 cells) were implanted into the tail of the pancreas. The pancreas was then placed back into the peritoneal cavity, and the peritoneum and skin were closed with suture and wound clips, respectively. Tumors were allowed to develop over 14–17 days to approximately 5 mm in diameter. Established tumors were irradiated in a single fraction (14–20 Gy) using the Small Animal Radiation Research Platform (SARRP). Anti-CCL2 (clone 2H5) neutralizing antibody, anti-Ly6C (clone Monts1) depleting antibody, hamster isotype control (hamster IgG), and rat isotype control (clone 2A3) were administered via intraperitoneal injection on days −1, 0, +1, and +3 of radiotherapy. Anti-CD4 (clone GK1.5) and anti-CD8 (clone 2.43) depleting antibodies were administered on day −1. All neutralizing and depleting antibodies were purchased from BioXcell and were endotoxin free. Every 3 to 4 days, the longest tumor dimension (L) and its perpendicular diameter (W) were measured using calipers; volume was calculated as $(L \times W^2)/2$. For survival studies, mice were euthanized when tumors reached 1,000 mm^3.

Histopathology and immunohistochemical analysis

Histopathology and IHC were performed on frozen tissue sections. Frozen sections were air dried and fixed with 3% formaldehyde. Hydrogen peroxide was used to quench endogenous peroxidases. Tissue was blocked with 10% normal goat serum in PBS with 0.1% Tween-20. Primary antibodies against mouse antigens included rat anti-F4/80 (eBioscience), rat anti-Ly6C (Abcam), rat anti-Ki67 clone TEC3 (Dako), rat anti-CD31 (BD Pharmingen), rat anti-CD45 (BD Pharmingen), and rabbit anti-cleaved caspase-3 (R&D Systems). Tissues were incubated in blocking buffer containing primary antibodies overnight at 4°C. After washing with PBS, tissues were incubated with PBS containing a secondary biotinylated goat anti-rat antibody (BD Pharmingen). Tissues were developed using Vectastain ABC Kit and counterstained with hematoxylin. Senescence-associated β-galactosidase staining was performed using the Senescence β-Galactosidase Staining Kit (Cell Signaling Technology). Fluorescent imaging was performed on an IX83 inverted microscope (Olympus) and bright-field images were acquired using a BX43 upright (Olympus) microscope.

Flow cytometry of subcutaneous tumors

Mice were euthanized, and subcutaneous tumors were harvested, measured, and weighed. Peritumoral lymph nodes were excluded from analysis. Tumors were minced at 4°C in digestion media containing collagenase (1 mg/mL, Sigma-Aldrich), DNase (150 U/mL, Roche), and Dispase (1 U/mL, Worthington), and then incubated at 37°C for 30 minutes with intermittent agitation. After 70-μm filtration and washing with PBS, single-cell suspensions were stained with antibodies in PBS containing 0.2 mmol/L EDTA with 2% FCS at 4°C for 15 minutes. Anti-mouse antibodies were purchased from BD Biosciences, unless stated otherwise: CD45 (30-F11, PE-Cy7), CD11b (BioLegend, M1/70, APC), F4/80 (eBiosciences; BM8, FITC), Ly6C (AL-21, APC-Cy7), Ly6G (1A8, Percp-Cy5.5), CCR2 (R&D Systems; clone #475301, PE). Antibody-stained single-cell suspensions were examined on a FACSCanto II (BD Biosciences) and analyzed using FlowJo

version 10 (FlowJo, LLC). For gene expression analysis of leukocyte subsets obtained from implanted tumors, antibody-stained single-cell suspensions were sorted on a FACSAria II (BD Biosciences) and RNA isolation was performed within 5 to 6 hours of the initial tumor digest. This protocol required 5×10^4 sorted cells per sample. Gating strategy for inflammatory monocytes (IM), granulocytes, and tumor-associated macrophages (TAM) is illustrated in Supplementary Fig. S1.

Cytokine analysis of tumor supernatant

For *in vivo* experiments, tumors were harvested, placed at 4°C in serum-free DMEM at 1 mg of tissue per 10 μL of media, and then minced. Tumor suspensions were centrifuged at 12,470 × *g* for 5 minutes, and supernatant was collected and stored at −20°C. For *in vitro* experiments, when tumor cell lines reached 70% to 80% confluence in 10-mm plates, cells were washed and incubated in fresh serum-free DMEM at 37°C; supernatant was then collected after 24 hours and stored at −20°C. Cytokines from *in vitro* and *in vivo* tumor supernatants were quantified using cytometric bead analysis (CBA; BD Biosciences), using references to recombinant murine standards.

Transwell migration assay

Bone marrow–derived cells (2×10^6/mL) from C57BL/6 mice were placed above a transwell membrane in DMEM containing 1% FCS, which was incubated in tumor supernatant collected *in vitro* as described above, in the presence or absence of a CCL2-neutralizing antibody (2H5, 10 ng/mL). After incubation at 37°C for 5 hours, transwell membranes were collected, fixed with formaldehyde, stained with crystal violet, and dried. Transmigrated cells were counted at 40× magnification using an upright bright-field microscope (Olympus BX43).

In vitro irradiation

PDAC cell lines at 70% to 80% confluence were cultured in DMEM containing 5% FCS at 0.5-cm depth and irradiated at a dose rate of 2.8 Gy/minute using the X-RAD 320ix (Precision X-ray, Inc.). Sham irradiation involved placing cell culture plates at a similar temperature for the length of irradiation.

RNA and gene expression array

Tumor tissue was processed and stored in TRIzol at −80°C. Tumor lysates were thawed on ice and allowed to equilibrate to room temperature before RNA was isolated using a Qiagen RNeasy Mini Kit, according to manufacturer's protocol. For *in vitro* experiments, tumor cells were washed and harvested using TRIzol. Flow-sorted samples were collected in TRIzol LS and RNA extraction was performed immediately. RNA was collected in RNase-free water and quantified using a NanoDrop Spectrophotometer. cDNA was synthesized from 1 μg of RNA per sample using MultiScribe Reverse Transcriptase and random hexamers (Applied Biosystems). Primers for qRT-PCR were designed using the Primer 3 online program (26, 27) and synthesized by Integrated DNA Technologies. SYBR Green chemistry (Applied Biosystems) was used to determine relative quantifications of all products; expression was normalized to β-actin and calculated using the ΔC_t formula. Fold change was calculated relative to the average of the control group. Primer sequences were as follows:

Murine Ccl2: forward 5′-AGCAGCAGGTGTCCCAAAGA-3′
Murine Ccl2: reverse 5′-GATCTCATTTGGTTCCGATCCA-3′
Human Ccl2: forward 5′-GAAGAATCACCAGCAGCAAGT-3′
Human Ccl2: reverse 5′-TCCTGAACCCACTTCTGCTT-3′

Microarray analysis

Microarray services were provided by the UPENN Molecular Profiling Facility, including quality control tests of the total RNA samples by Agilent Bioanalyzer and Nanodrop spectrophotometry. All protocols were conducted as described in the NuGEN Ovation Pico WTA system v2 user guide and the Affymetrix GeneChip Expression Analysis Technical Manual. Briefly, 25 ng of total RNA was converted to first-strand cDNA using reverse transcriptase primed by poly(T) and random oligomers that incorporated an RNA priming region. Second-strand cDNA synthesis was followed by ribo-SPIA linear amplification of each transcript using an isothermal reaction with RNase, RNA primer, and DNA polymerase, and the resulting ssDNA was assessed by Bioanalyzer, fragmented, and biotinylated by terminal transferase end labeling. Labeled cDNA (5.5 μg) were added to Affymetrix hybridization cocktails, heated at 99°C for 5 minutes and hybridized for 16 hours at 45°C to Mouse Gene 2.0 ST GeneChips (Affymetrix Inc.) using the GeneChip Hybridization oven 645. The microarrays were then washed at low (6× SSPE) and high (100 mmol/L MES, 0.1 mol/L NaCl) stringency and stained with streptavidin–phycoerythrin. Fluorescence was amplified by adding biotinylated anti-streptavidin and an additional aliquot of streptavidin–phycoerythrin stain. A GeneChip 3000 7G scanner was used to collect fluorescence signal. Affymetrix Command Console and Expression Console were used to quantitate expression levels for targeted genes; default values provided by Affymetrix were applied to all analysis parameters. Heatmaps were generated using GENE-E matrix visualization and analysis platform. Gene expression data is available through the NCBI GEO database (accession number GSE82276).

CRISPR knockout

Oligonucleotides (GCAAGATGATCCCAATGAGT and GGCC TGCTGTTCACAGTTGC, Integrated DNA Technologies) encoding guide RNAs that target murine CCL2 exons were cloned into TOPO-expression vectors (Life Technology). A clonal tumor line, derived from a parental KPC-derived PDAC cell line, was then cotransfected using 5 μg LentiCRISPR V2 plasmid (Addgene) with 5 μg of TOPO-CCL2 gRNA plasmids or a control vector targeting GFP. One day after transfection, transfected cells were selected for 48 hours with 10 ng/mL puromycin. Isogenic clones of transfected cells were isolated to produce clonal lines, in which CCL2 knockout was confirmed by cytometric bead array (CBA; BD Biosciences) of tumor cell supernatant.

Statistical analysis

Statistical significance was determined by Student *t* test performed with or without Welch correction for unequal variance using GraphPad Prism Version 6.05 (GraphPad Software, Inc.). Significance testing for tumor growth over time was performed using repeated measures two-way ANOVA with Tukey multiple comparisons of means as a *post hoc* test to evaluate differences between two groups. In some cases, tumor volumes were compared at each time point using Student *t* test with Holm–Šídák method to correct for multiple comparisons. Significance of overall survival was determined using log-rank analysis.

Results

Ablative radiotherapy minimally affects PDAC tumor growth

To investigate the impact of ablative radiotherapy in an immunologically resistant tumor model (21), we derived PDAC cell lines from tumors arising spontaneously in KPC mice and injected them subcutaneously into syngeneic C57BL/6 mice. Approximately 2 weeks later, established tumors were treated with 20 Gy ablative radiotherapy, a dose that is comparable with that used clinically for human PDAC (13). Similar to results reported in patients with PDAC, we found that a single dose of radiotherapy only partially delayed tumor growth (Fig. 1A). However, in contrast to findings in immunogenic murine melanoma and colon cancer models (18, 28), depletion of $CD4^+$ and $CD8^+$ T cells did not have an impact on the delay in tumor growth induced by radiotherapy (Fig. 1A). Furthermore, we observed no significant difference in T-cell infiltration into tumors after radiotherapy (Supplementary Fig. S2). These findings revealed that ablative radiotherapy alone is insufficient to invoke a productive antitumor immune response against an immunologically resistant tumor such as PDAC.

PDAC tumors respond to ablative radiotherapy by releasing chemokines including CCL2

To investigate potential immune mechanisms regulating the efficacy of ablative radiotherapy, we next examined the intratumoral cytokine profile induced by radiotherapy. At baseline, tumors demonstrated high levels of CCL2, MIG, and G-CSF among a panel of cytokines (Fig. 1B), which is consistent with the robust inflammatory response seen in PDAC (29). However, after radiotherapy, there were small but significant

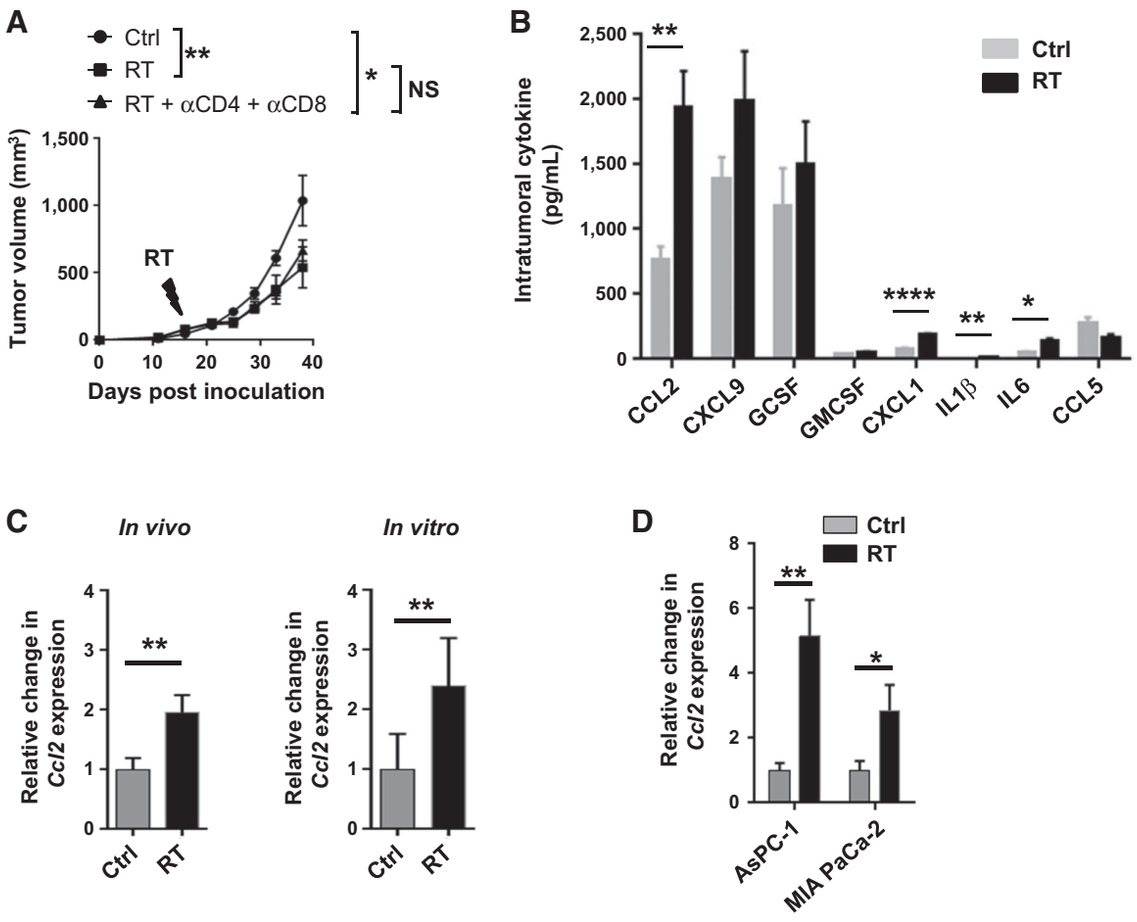

Figure 1.

Radiotherapy (RT) resistance in PDAC is associated with increased production of tumor-derived CCL2. **A,** Tumor growth curve of a KPC-derived PDAC cell line (152.PDA) implanted subcutaneously and treated on day 16 after implantation with radiotherapy (20 Gy) or sham (Ctrl) in combination with CD4 and CD8 T-cell depleting antibodies compared with isotype controls. Shown is mean ± SEM, $n = 5$ mice per group. Tumor growth was compared using repeated measure two-way ANOVA ($P < 0.05$) with Tukey multiple comparisons of means to evaluate differences between two groups. **B,** Bar graph displaying intratumoral cytokine and chemokine levels (pg/mL) detected 24 hours after sham (Ctrl) or radiotherapy (20 Gy). **C,** Fold change in *Ccl2* expression detected within tumors *in vivo* and *in vitro* 3 days after radiotherapy (20 Gy) compared with sham (Ctrl). *Ccl2* expression was normalized to *β-actin*. **D,** Fold change in *CCL2* expression detected in human PDAC cell lines AsPC-1 and MIA PaCa-2 at 3 days after radiotherapy compared with sham (Ctrl). For each treatment group, *CCL2* expression was normalized to GAPDH. Significance testing was performed using unpaired two-tailed Student *t* test. *, $P < 0.05$; **, $P < 0.01$; ***, $P < 0.001$; ****, $P < 0.0001$.

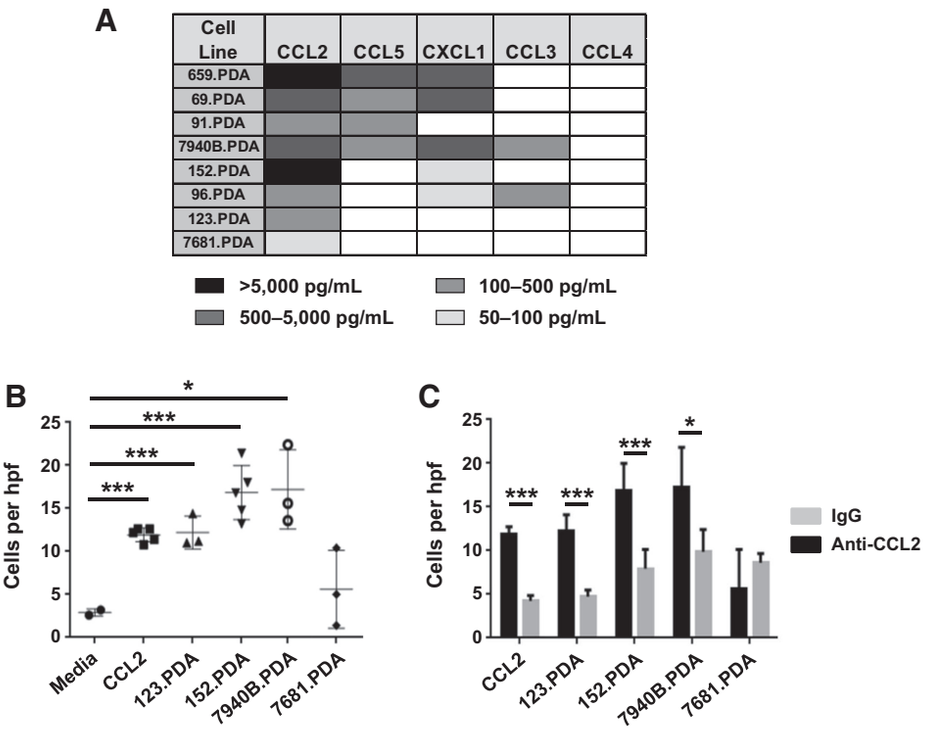

Figure 2.
PDAC-derived CCL2 induces myeloid cell migration. **A,** Heatmap displaying chemokine production by KPC-derived PDAC cell lines grown *in vitro*. **B,** Migration of bone marrow–derived cells in response to tumor-derived soluble factors from indicated cell lines with comparison to CCL2 (10 ng/mL) and media alone. **C,** Shown is the impact of anti-CCL2 neutralizing antibodies versus isotype control (IgG) on bone marrow–derived cell migration induced by tumor-derived soluble factors from indicated cell lines or CCL2 (10 ng/mL). For **B** and **C,** migrated cells were quantified at 40× magnification (hpf). Significance testing was performed using unpaired two-tailed Student *t* test. *, $P < 0.05$; **, $P < 0.01$; ***, $P < 0.001$; ****, $P < 0.0001$.

increases in the levels of CXCL1, IL1β, and IL6. Most notably, although, there was a marked increase in CCL2 ($\Delta = 1{,}178 \pm 294$ pg/mL; Fig. 1B). This increase in CCL2 levels in response to radiotherapy was also seen at the RNA level (Fig. 1C) and was reproducible using a second KPC-derived PDAC cell line *in vivo* (Supplementary Fig. S3).

We next examined the capacity of tumor cells to secrete CCL2 in response to radiotherapy. We found that *Ccl2* expression increased *in vitro* in response to radiotherapy (Fig. 1C), suggesting that tumor cells, not just stromal or immune cells, likely contribute to the increase in CCL2 within the tumor microenvironment. This same radiotherapy-induced CCL2 release was also seen with two human PDAC cell lines. Here, radiotherapy augmented *CCL2* expression in both MIA PaCa-2 and AsPC-1 human PDAC cell lines by 2.8 ± 0.5-fold and 5.1 ± 0.8-fold, respectively (Fig. 1D). Thus, PDAC responds to radiotherapy by releasing CCL2.

PDAC-derived CCL2 regulates migration of bone marrow–derived cells

Consistent with clinical data suggesting that CCL2 expression is increased in human PDAC (30), we detected high levels of CCL2 produced *in vitro* by an array of KPC-derived PDAC cell lines. In contrast, other chemokines important for the recruitment of myeloid cells, such as CCL5, CXCL1, CCL3, and CCL4, were not uniformly detected (Fig. 2A).

We next used an *in vitro* chemotaxis assay to understand the significance of tumor-derived factors in recruiting myeloid cells to the tumor microenvironment. We found that soluble factors produced by PDAC cell lines induced the migration of bone marrow–derived cells across a transwell membrane (Fig. 2B). The magnitude of cell migration induced by PDAC was comparable with myeloid cell migration toward 10 ng/mL CCL2 (Fig. 2B). Furthermore, bone marrow–derived cells that migrated across the transwell membrane were enriched for CCR2 expression (Supplementary Fig. S4). To determine the role of tumor-derived CCL2 in directing myeloid cell chemotaxis, we neutralized CCL2 *in vitro* using a CCL2-specific antibody and found a significant reduction in the migration of bone marrow–derived cells (Fig. 2C) demonstrating a major role for PDAC-derived CCL2 for myeloid cell chemotaxis.

Ablative radiotherapy induces tumor recruitment of CCR2-expressing inflammatory monocytes/macrophages *in vivo*

Given the effect of ablative radiotherapy on intratumoral chemokine levels, we examined the dynamics of myeloid cell composition within the tumor microenvironment after radiotherapy. By H&E staining, we detected an increase in cellular content 3 days after radiotherapy, suggesting an acute inflammatory response (Fig. 3A). On more detailed examination of the immune microenvironment, we detected an increase in the frequency of $F4/80^+$ monocytes/macrophages within tumors (Fig. 3B). Using flow cytometry, we also found an increase in leukocytes as a percentage of live cells within tumors after radiotherapy (Fig. 3C). Specifically, we observed an increase in TAMs ($CD45^+CD11b^+Ly6C^{lo}F4/80^+$) and inflammatory monocytes/macrophages ($CD45^+CD11b^+Ly6C^{hi}$). In contrast, we detected no change in granulocyte ($CD45^+CD11b^+Ly6G^+$) recruitment. Similar findings were observed in an orthotopic model of PDAC, where ablative radiotherapy induced an increase in inflammatory monocytes/macrophages without a change in granulocyte infiltration (Supplementary Fig. S5).

The increase in inflammatory monocyte/macrophage infiltration seen after radiotherapy was consistent with the increase in intratumoral CCL2 levels induced by radiotherapy (Fig. 1). Inflammatory monocytes/macrophages express

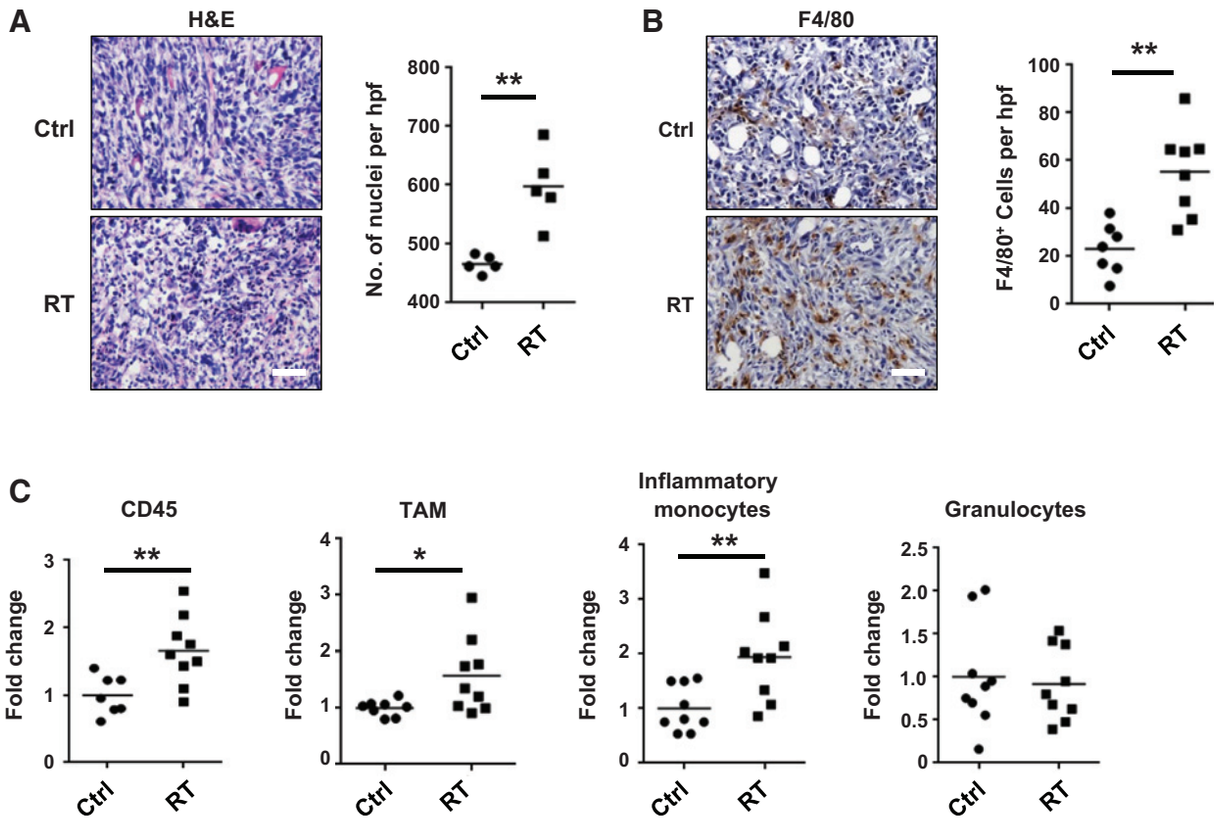

Figure 3.

Radiotherapy (RT) enhances myeloid cell recruitment to the tumor microenvironment in PDAC. **A,** Representative images of H&E staining of PDAC tumors (152.PDA) at 3 days after treatment with radiotherapy (20 Gy) versus sham. Nuclei are quantified as a measure of cellularity. **B,** Representative images of F4/80 immunostaining of PDAC tumors (152.PDA) at 3 days after treatment with radiotherapy (20 Gy) versus sham (Ctrl). F4/80$^+$ cells are quantified. For **A** and **B,** images are taken at 40× magnification (hpf) and scale bar represents 50 μm. **C,** Leukocyte subsets within tumors at 3 days after radiotherapy (20 Gy) versus sham (Ctrl). Shown are the fold changes of total CD45$^+$ cells, tumor-associated macrophages (TAM, CD45$^+$CD11b$^+$F480$^+$Ly6C^{lo}), inflammatory monocytes (CD45$^+$CD11b$^+$F4/80$^+$Ly6C^{hi}), and granulocytes (CD45$^+$CD11b$^+$F4/80^{neg}Ly6G$^+$) as a percentage of total live cells. Fold change is calculated relative to the average of the control group. Each data point represents a single mouse. Significance testing was performed using unpaired two-tailed Student *t* test. *, $P < 0.05$; **, $P < 0.01$.

CCR2, the receptor for CCL2, which can direct both the egress of immature inflammatory monocytes from the bone marrow into the peripheral blood and their subsequent infiltration into tissues (24, 31). Therefore, we hypothesized that inflammatory monocytes/macrophages may respond to radiation-induced injury by acquiring an altered phenotype that regulates the efficacy of ablative radiotherapy. To test this hypothesis, we examined the gene expression profile of flow-sorted inflammatory monocytes/macrophages isolated from tumors 1 day after ablative radiotherapy compared with control tumors. This analysis revealed only eight of 34,365 transcripts that reached a predetermined threshold of twofold change in expression with a <25% FDR (Supplementary Fig. S6). Four of these, including *Phlda3*, *Ccna1*, *Ddias*, and *Trp53inp1* are recognized as cell-cycle or stress response genes. However, none of these genes is known as major determinants of cellular phenotype to suggest a role in redirecting the biology of tumor-infiltrating monocytes/macrophages. Therefore, the minimal impact of ablative radiotherapy on the gene expression profile of inflammatory monocytes/macrophages supports a role for radiotherapy primarily in altering the quantity rather than the quality of inflammatory monocytes/macrophages recruited to the tumor microenvironment.

CCL2 neutralization delays tumor regrowth after radiotherapy by impeding inflammatory monocyte recruitment

CCL2 expression and inflammatory monocyte recruitment have been implicated as poor prognostic factors in a variety of malignancies (30, 32, 33). We hypothesized that radiotherapy-induced expression of CCL2 within the tumor microenvironment may recruit inflammatory monocytes/macrophages and TAMs to promote resistance to ablative radiotherapy. To test this hypothesis, mice bearing established PDAC tumors injected subcutaneously were treated with a neutralizing antibody to CCL2 (or control) on days −1, 0, +1, and +3 relative to radiotherapy versus sham treatment. Compared to radiotherapy alone, the combination of radiotherapy and a CCL2-neutralizing antibody significantly impacted tumor growth and prolonged survival (Fig. 4A). This effect was reproduced using a second KPC-derived PDAC cell line (Supplementary Fig. S7).

Although some tumor cells have been reported to express CCR2, we found that CCR2 expression within PDAC tumors was

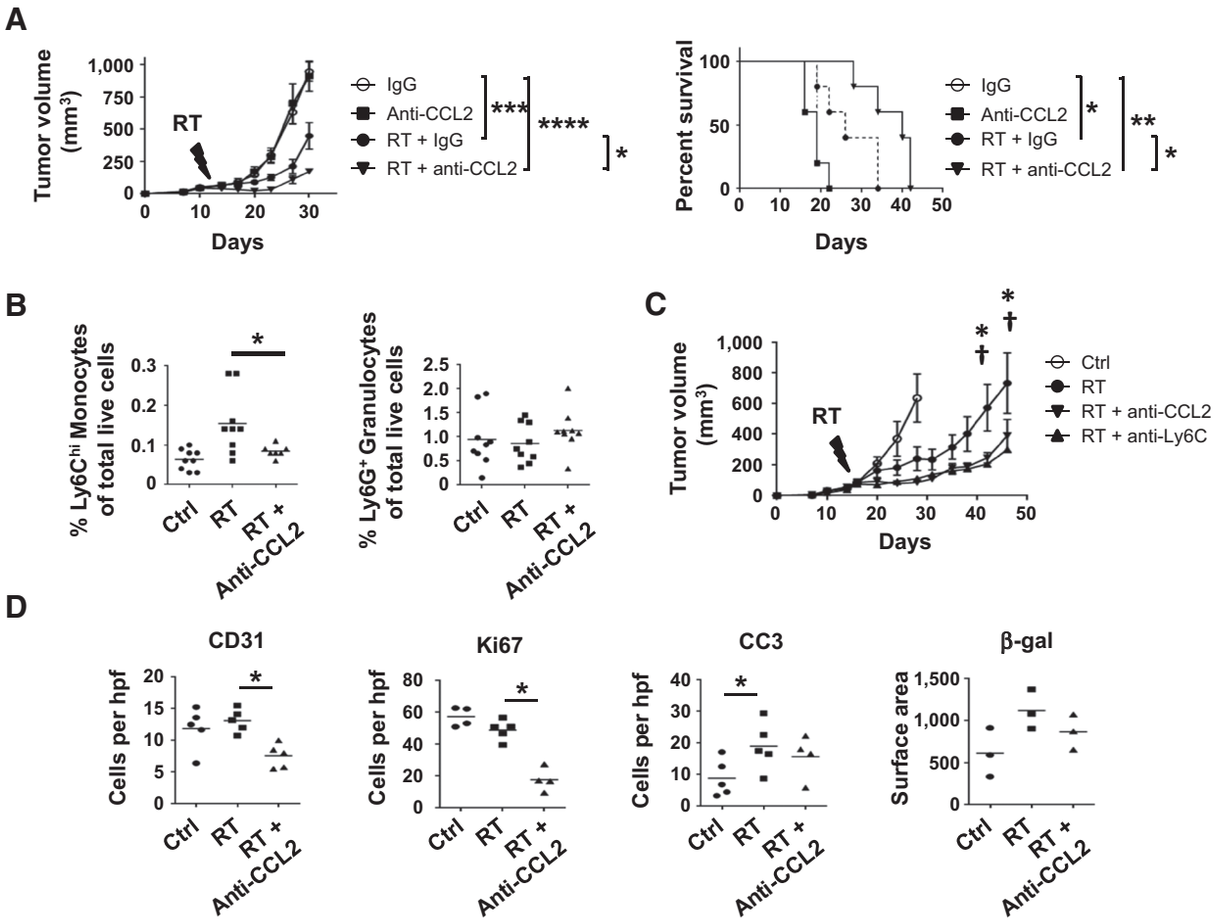

Figure 4.

CCL2 neutralization inhibits radiotherapy (RT)-induced recruitment of inflammatory monocytes to PDAC and enhances radiotherapy efficacy. Established PDAC tumors (152.PDA) implanted into syngeneic mice were treated with radiotherapy (14 Gy) or sham. Anti-CCL2 neutralizing antibodies, anti-Ly6C depleting antibodies, or isotype control were administered on days −1, 0, 1, and 3 of radiotherapy. **A,** Tumor growth curve and Kaplan–Meier survival plot showing impact of CCL2 neutralizing antibodies on radiotherapy efficacy. Significance testing for tumor growth over time was performed using repeated measures two-way ANOVA ($P < 0.0001$) with Tukey multiple comparisons of means as a *post hoc* test to evaluate differences between two groups. Survival significance was tested using log-rank analysis. **B,** Shown are percentages of Ly6C^{hi} inflammatory monocytes and Ly6G^{+} granulocytes of total live cells detected within tumors at 3 days after radiotherapy (20 Gy), versus sham (Ctrl), with or without anti-CCL2 neutralizing antibodies. Each data point represents a single mouse. **C,** Tumor growth curve showing impact of anti-CCL2 and anti-Ly6C antibodies on radiotherapy efficacy. Significance testing was performed at each time point using Student *t* test with Holm–Šidák method to correct for multiple comparisons. *, $P < 0.05$ for radiotherapy versus radiotherapy + anti-CCL2; †, $P < 0.05$ for radiotherapy versus radiotherapy + anti-Ly6C. Data from **A** and **C** are representative of at least five and two independent experiments, respectively. **D,** Quantification of immunohistochemical staining for vascularity (CD31), proliferation (Ki67), apoptosis (cleaved caspase-3), and senescence (β-galactosidase). Immunostains were quantified at 40× magnification (hpf). Each data point represents a single mouse. For **B** and **D,** significance testing was performed using unpaired two-tailed Student *t* test. *, $P < 0.05$; **, $P < 0.01$; ***, $P < 0.001$; ****, $P < 0.0001$.

limited to a subset of CD45^{+} leukocytes (Supplementary Fig. S8). In addition, CCL2 neutralization alone did not impact tumor growth (Fig. 4A). Therefore, to understand the impact of CCL2 neutralization on the efficacy of radiotherapy, we examined the myeloid compartment of tumors 3 days after radiotherapy. We found that the acute increase in inflammatory monocytes induced by radiotherapy was abrogated by CCL2 neutralization *in vivo* (Fig. 4B). In contrast, the presence of granulocytes within tumors was not affected by radiotherapy or the combination of radiotherapy and CCL2 neutralization (Fig. 4B).

Our findings with CCL2 neutralization suggested a key role for inflammatory monocytes/macrophages as an immune resistance mechanism to ablative radiotherapy in PDAC. To further address this possibility, we depleted Ly6C^{hi} inflammatory monocytes/macrophages using a Ly6C-depleting antibody (24). Using this approach, we found that depletion of inflammatory monocytes significantly delayed tumor growth after radiotherapy, and mirrored the impact of CCL2 neutralization (Fig. 4C). To understand the mechanism by which inflammatory monocytes promote tumor growth after radiotherapy, we examined tumor specimens by IHC. After radiotherapy alone there was no change in vascularity or proliferation, but increased apoptosis (cleaved caspase-3) and a trend toward increased senescence (Fig. 4D). Compared with radiotherapy alone, we found that the combination of

radiotherapy and CCL2 neutralization significantly reduced tumor vascularity (decrease in $CD31^+$ cells per high-power field) and proliferation (decreased $Ki67^+$ cells per high-power field) without further having an impact on apoptosis (cleaved caspase-3) or senescence (β-galactosidase; Fig. 4D). Furthermore, in contrast to immunogenic cancer models where CCL2 neutralization can induce T-cell infiltration, we found that CCL2 neutralization with or without radiotherapy failed to lead to recruitment of $CD3^+$ T cells to the tumor microenvironment (Supplementary Fig. S9). Thus, PDAC responds to ablative radiotherapy by releasing CCL2, which then recruits inflammatory monocytes/macrophages to support tumor proliferation and vascularization.

Tumor-derived CCL2 limits efficacy of ablative radiotherapy in PDAC

Both malignant and nonmalignant cells can secrete CCL2 within the tumor microenvironment. In a breast cancer metastasis model, CCL2 produced by both malignant and nonmalignant cells was found to be important for recruiting inflammatory monocytes/macrophages to promote metastasis (32). However, our findings in models of PDAC demonstrate that malignant cells respond to ablative radiotherapy by significantly increasing CCL2 production. This raised the possibility that CCL2 produced by malignant cells may be the main mediator of immune resistance to radiotherapy. Therefore, we next examined the role of tumor-derived CCL2 in promoting resistance to radiotherapy. To do this, we genetically eliminated CCL2 from a clonal KPC-derived PDAC cell line using CRISPR technology. As expected, compared with the wild-type clonal cell line ($CCL2^{wt}$), the $CCL2^{null}$ cell line did not produce CCL2 (Fig. 5A). We next examined the biology of $CCL2^{null}$ versus $CCL2^{wt}$ tumors implanted into syngeneic mice. We found that levels of CCL2 were significantly decreased in $CCL2^{null}$ PDAC tumors, although not completely eliminated (Fig. 5A), which likely represents nonmalignant sources of CCL2. In contrast, we did not observe any difference in the engraftment or outgrowth

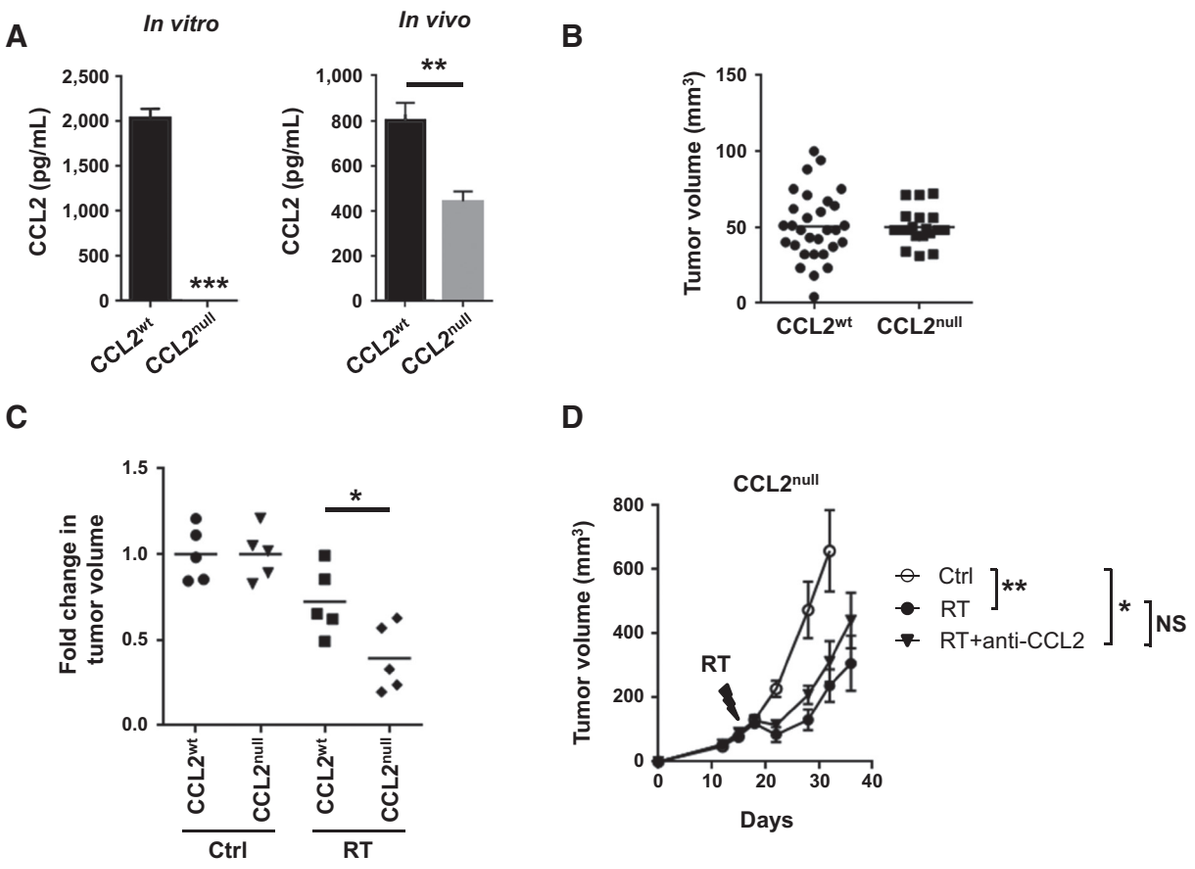

Figure 5.

Tumor-derived CCL2 regulates radiotherapy (RT) efficacy in PDAC. CRISPR technology was used to knockout CCL2 in PDAC cells. **A,** Shown is CCL2 (pg/mL) produced by wild-type PDAC cells ($CCL2^{wt}$) and CCL2-knockout PDAC cells ($CCL2^{null}$) *in vitro* and *in vivo*. **B,** Tumor volume of $CCL2^{wt}$ and $CCL2^{null}$ PDAC cell lines at 12 days after implantation. Each data point represents a single mouse. **C,** Fold change in tumor volume 4 days after ablative radiotherapy (14 Gy) in control ($CCL2^{wt}$) and $CCL2^{null}$ clonal PDAC cell lines, relative to baseline. Data were normalized to untreated controls. **D,** Tumor growth curve for $CCL2^{null}$ PDAC cells treated with radiotherapy (14 Gy), versus sham (Ctrl), with or without anti-CCL2 neutralizing antibodies. Shown is mean ± SEM; $n = 5$ mice per group. Data are representative of 2 independent experiments. For **A–C,** significance testing was performed using unpaired two-tailed Student *t* test. For **D,** significance testing for tumor growth over time was determined using repeated measures two-way ANOVA ($P < 0.0001$) with Tukey multiple comparisons of means as a *post hoc* test to evaluate differences between two groups. *, $P < 0.05$; **, $P < 0.01$; ***, $P < 0.001$.

of CCL2^{null} compared with CCL2^{wt} tumors (Fig. 5B). Finally, we determined the capacity of radiotherapy to have an impact on the *in vivo* growth of CCL2^{null} versus CCL2^{wt} tumors *in vivo*. We found that the responsiveness of CCL2^{null} tumors to radiotherapy was significantly increased compared with CCL2^{wt} tumors as seen by deeper tumor regressions (Fig. 5C). In addition, consistent with the importance of tumor-derived CCL2 in regulating the efficacy of ablative radiotherapy, CCL2 neutralization did not improve radiotherapy efficacy in CCL2^{null} tumors (Fig. 5D), as had been seen in CCL2-expressing tumors (Fig. 4A). Together, our findings support a role for tumor-derived CCL2 as a key mechanism of resistance to ablative radiotherapy in PDAC.

Discussion

Local disease progression can be a major complication of unresectable PDAC with patients developing (i) sepsis secondary to biliary obstruction, (ii) hemorrhage and bowel obstruction related to duodenal invasion, and (iii) intractable pain from celiac plexus involvement. Overall, nearly one-third of patients with PDAC will die from uncontrolled local disease (3). Although radiotherapy remains a mainstay for disease control in the locally advanced setting, human PDAC has demonstrated significant resistance to radiotherapy. This resistance has been attributed to an inherent radioresistance of tumor cells, increased hypoxia, poor vascularity, and dense fibrosis (34–37). Our findings now identify a novel mechanism of radiotherapy resistance wherein PDAC cells appear inherently programmed to respond to radiotherapy-induced stress by releasing high levels of CCL2 that recruit inflammatory monocytes to promote tumor proliferation and vascularity (Fig. 6). Thus, our data support a role for CCL2-dependent inflammation as a major checkpoint to the efficacy of radiotherapy in PDAC.

In this study, we found that ablative radiotherapy, although limited in its antitumor efficacy, induced the accumulation of chemokines and cytokines within the tumor microenvironment, in particular, CCL2. Although chemokine production within the tumor microenvironment can be driven by both malignant and nonmalignant cells, *in vitro* studies of murine and human PDAC cell lines showed that tumor cells respond to the stress of ablative radiotherapy by augmenting CCL2 expression. Tumor-derived CCL2 was found to be critical for inducing chemotaxis of inflammatory monocytes and directed the recruitment of inflammatory monocytes/macrophages and TAMs to the tumor microenvironment. We found that selective blockade of inflammatory monocyte recruitment, although ineffective alone, improved the antitumor effect of ablative radiotherapy and prolonged survival in a murine model of PDAC. This approach was contingent on tumor-derived CCL2 expression. Using cell lines in which CCL2 was genetically deleted, we observed that tumor-derived CCL2 was necessary for the antitumor effect of CCL2 neutralization in combination with radiotherapy, despite continued expression of CCL2 by nonmalignant cells within the tumor microenvironment. This finding suggests that the proximity of inflammatory monocytes/macrophages to tumor cells which may be directed by tumor-derived CCL2 is critical for monocyte/macrophage protumor activity in the setting of radiotherapy (38).

Using a poorly immunogenic model of PDAC, we found that T cells were not required for CCL2 neutralization to improve the efficacy of ablative radiotherapy. Rather, our findings demonstrate that CCL2 neutralization inhibits inflammatory monocyte recruitment to tumors and their subsequent role in supporting tumor recovery from the cytotoxic effects of radiotherapy. This finding contrasts the use of CCL2–CCR2 blockade in other more immunogenic tumors, where it has been shown to induce T-cell–dependent antitumor immunity when administered in combination with cytotoxic chemotherapy (30, 33). In addition, our findings contrast recent reports in immunogenic cancer models describing a role for T cells in the antitumor effects of ablative radiotherapy (18, 28). These distinct outcomes observed with ablative radiotherapy across immunogenic and poorly immunogenic models suggest a role for baseline tumor immunogenicity in defining rational therapeutic combinations with radiotherapy. As the PDAC tumor microenvironment commonly excludes effector T cells, therapeutic strategies that combine ablative radiotherapy with T-cell–based therapies such as immune checkpoint blockade may be unlikely to be effective without first restoring productive T-cell immunosurveillance, such as with vaccines (39). Our findings in a poorly immunogenic model of PDAC demonstrate that ablative radiotherapy alone is insufficient to overcome T-cell exclusion and, thus, is unlikely to potentiate the activity of immunotherapies that rely on a preexisting T-cell response.

Inflammatory monocytes and the CCL2–CCR2 axis are commonly associated with a poor prognosis in several malignancies,

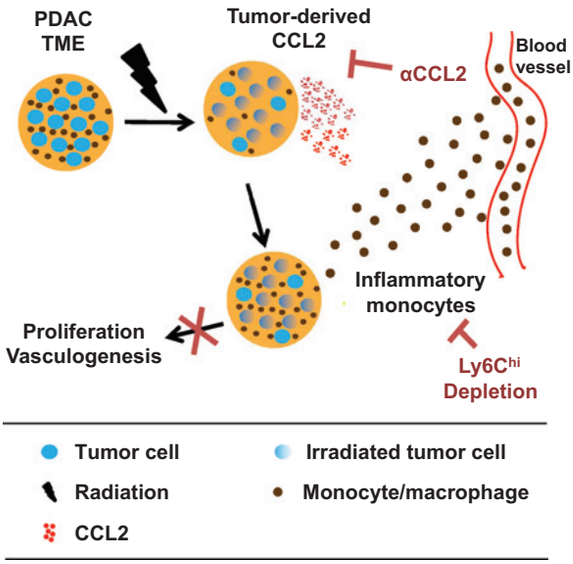

Figure 6.

Conceptual model describing a role for monocytes and CCL2 in PDAC resistance to radiotherapy (RT). The PDAC tumor microenvironment (TME) consists of tumor cells (blue), leukocytes (brown) including macrophages and their precursor monocytes, and other nonmalignant stromal cells including fibroblasts and endothelial cells (not shown). Ablative radiotherapy results in cell death in a fraction of tumor cells and leukocytes within the TME. PDAC cells respond to radiotherapy by increasing their production of chemokines, including CCL2, which acts to recruit CCR2^{+} inflammatory monocytes to the TME. Tumor-infiltrating monocytes/macrophages then support tumor proliferation and neovascularization and therein establish PDAC resistance to radiotherapy. Neutralization of CCL2 or depletion of Ly6C^{hi} inflammatory monocytes blocks radiotherapy-induced monocyte/macrophage recruitment to tumors and their subsequent protumor effects leading to enhanced radiotherapy efficacy.

including PDAC, hepatocellular carcinoma, and breast cancer (30, 32, 33). Our findings suggest that radiotherapy does not alter the phenotype of tumor-infiltrating monocytes/macrophages but rather enhances their recruitment to the tumor microenvironment. We performed this analysis on tumor-infiltrating monocytes 1 day after radiotherapy reasoning that an early time point would be necessary to capture changes in gene expression prior to their differentiation within the tumor microenvironment. Under basal conditions, inflammatory monocytes/macrophages appear to comprise a small subset of leukocytes in the PDAC microenvironment, but unlike granulocytes and TAMs, this subset expresses the chemokine receptor CCR2. Inflammatory monocytes recruited to the tumor microenvironment in a CCL2–CCR2-dependent manner can undergo rapid differentiation into TAMs and in doing so, lose Ly6C expression. This is consistent with inflammatory monocytes/macrophages as precursors of TAMs and implies that their recruitment to the tumor microenvironment in response to ablative radiotherapy may help reconstitute the myeloid compartment. However, the transient nature of Ly6C expression may lead to an underestimation of the magnitude of this recruitment when examined on a quantitative basis.

We have shown a therapeutic role for inhibiting monocyte infiltration into tumors after ablative radiotherapy. However, the robust innate immune response that is induced by radiotherapy within tumors also raises the possibility that this immune reaction may be redirected with antitumor activity. For example, IFNγ released systemically in response to a CD40 agonist can redirect tumor-infiltrating monocytes with antifibrotic and antitumor properties (19, 24). Thus, we propose that combining radiotherapy with immune adjuvants may be one way to harness the inflammatory response invoked by ablative radiotherapy.

The myeloid response to cancer is inherently pliable with its phenotype dependent on local signals received within the tumor microenvironment. Our findings show that this myeloid response is a key determinant of tumor cell survival and resilience to radiotherapy. In our study, we demonstrate that modulating ablative radiotherapy-induced inflammation using CCL2-neutralizing antibodies can enhance the efficacy of radiotherapy. These findings support targeting the CCL2–CCR2 axis in combination with ablative radiotherapy to improve local disease control in patients with locally advanced PDAC. This translational approach may have particular promise in patients with genetic signatures that suggest a more locally invasive disease phenotype (40).

Our study was mainly conducted in a subcutaneous model of PDAC using KPC-derived cell lines. Although there may be differences in the efficacy of ablative radiotherapy in PDAC depending on the anatomical location of the treated tumor, we have found that ablative radiotherapy can induce inflammatory monocyte recruitment into PDAC tumors irrespective of whether they were implanted subcutaneously or orthotopically. Nonetheless, it is possible that PDAC tumors arising spontaneously may establish a microenvironment that is distinct from tumors implanted subcutaneously or orthotopically. Our study does not address this possibility given current technical limitations in delivering focal image-guided radiotherapy to abdominal tumors in mice. However, this is not a limitation to treating patients with locally invasive pancreatic tumors where conformal techniques for delivering ablative doses of radiotherapy are well established.

Multiple CCL2 and CCR2 antagonists have been developed and their clinical investigation is ongoing (33, 41–43). However, efforts to combine these agents with radiotherapy have not yet been explored. In contrast, agents targeting the CCL2–CCR2 axis in PDAC are actively under investigation in combination with cytotoxic chemotherapy and early results appear promising (44). The efficacy of chemotherapy in PDAC, although, is limited by the dense fibrotic reaction that surrounds PDAC, whereas ablative doses of radiotherapy can be effectively delivered to produce potent cell injury that is associated with a robust inflammatory response. Thus, combining CCL2/CCR2 antagonists with ablative radiotherapy may be particularly effective at enhancing the efficacy of radiotherapy and warrants clinical investigation based on our findings.

In summary, CCL2 plays an important role in the myeloid response to ablative radiotherapy in PDAC, a tumor that is inherently poorly immunogenic. Our data demonstrate that ablative radiotherapy induces tumor-derived CCL2 expression, which drives recruitment of inflammatory monocytes and macrophages into the tumor microenvironment to promote resistance to radiotherapy (Fig. 6). We propose that inhibition of inflammatory monocyte recruitment, by antagonizing the CCL2–CCR2 chemokine axis in combination with ablative radiotherapy, is a novel therapeutic approach for improving disease control in PDAC, where local tumor growth is responsible for significant morbidity and mortality.

Disclosure of Potential Conflicts of Interest

No potential conflicts of interest were disclosed.

Authors' Contributions

Conception and design: A. Kalbasi, G.M. Tooker, E. Ben-Josef, G.L. Beatty
Development of methodology: A. Kalbasi, G.M. Tooker, M. Liu, G.L. Beatty
Acquisition of data (provided animals, acquired and managed patients, provided facilities, etc.): A. Kalbasi, C. Komar, G.M. Tooker, M. Liu, J.W. Lee, W.L. Gladney, G.L. Beatty
Analysis and interpretation of data (e.g., statistical analysis, biostatistics, computational analysis): A. Kalbasi, C. Komar, G.M. Tooker, M. Liu, E. Ben-Josef, G.L. Beatty
Writing, review, and/or revision of the manuscript: A. Kalbasi, C. Komar, G.M. Tooker, M. Liu, J.W. Lee, W.L. Gladney, E. Ben-Josef, G.L. Beatty
Administrative, technical, or material support (i.e., reporting or organizing data, constructing databases): A. Kalbasi, G.L. Beatty
Study supervision: G.L. Beatty

Acknowledgments

We thank Kristen B. Long and Ioannis I. Verginadis for technical assistance and helpful discussions; W. Tim Jenkins and Cameron J. Koch for assistance with the Small Animal Radiation Research Platform; and Adam Bedenbaugh for assistance with frozen sectioning of tumors.

Grant Support

This work was supported by a Conquer Cancer Foundation of ASCO Young Investigator Award (to A. Kalbasi), NIH grants K08 CA138907 (to G. L. Beatty), F30 CA196106 (to J.W. Lee), and F30 CA196124 (to M. Liu), Abramson Cancer Center-Radiation Oncology Joint Pilot Award (to A. Kalbasi, E. Ben-Josef, and G. L. Beatty), and Damon Runyon Cancer Research Foundation for which G. L. Beatty is Nadia's Gift Foundation Innovator of the Damon Runyon-Rachleff Innovation Award (DRR-15-12).

The costs of publication of this article were defrayed in part by the payment of page charges. This article must therefore be hereby marked *advertisement* in accordance with 18 U.S.C. Section 1734 solely to indicate this fact.

Received April 5, 2016; revised June 16, 2016; accepted June 23, 2016; published OnlineFirst June 28, 2016.

References

1. Ryan D, Hong T, Bardeesy N. Pancreatic adenocarcinoma. N Engl J Med 2014;371:1039–49.
2. American Cancer Society. Cancer facts & figures 2016. Atlanta, Georgia: American Cancer Society; 2016.
3. Iacobuzio-Donahue CA, Fu B, Yachida S, Luo M, Abe H, Henderson CM, et al. DPC4 gene status of the primary carcinoma correlates with patterns of failure in patients with pancreatic cancer. J Clin Oncol 2009;27:1806–13.
4. Wyse JM, Carone M, Paquin SC, Usatii M, Sahai AV. Randomized, double-blind, controlled trial of early endoscopic ultrasound-guided celiac plexus neurolysis to prevent pain progression in patients with newly diagnosed, painful, inoperable pancreatic cancer. J Clin Oncol 2011;29:3541–6.
5. Moss AC, Morris E, Mac Mathuna P. Palliative biliary stents for obstructing pancreatic carcinoma. Cochrane Database Syst Rev 2006; CD004200.
6. Jeurnink SM, Steyerberg EW, van Hooft JE, van Eijck CHJ, Schwartz MP, Vleggaar FP, et al. Surgical gastrojejunostomy or endoscopic stent placement for the palliation of malignant gastric outlet obstruction (SUSTENT study): a multicenter randomized trial. Gastrointest Endosc 2010;71:490–9.
7. Konstantinidis IT, Warshaw AL, Allen JN, Blaszkowsky LS, Fernandez-del Castillo C, Deshpande V, et al. Pancreatic ductal adenocarcinoma: is there a survival difference for R1 resections versus locally advanced unresectable tumors? What is a "true" R0 resection? Ann Surg 2013; 257:731–6.
8. Murphy JD, Adusumilli S, Griffith KA, Ray ME, Zalupski MM, Lawrence TS, et al. Full-dose gemcitabine and concurrent radiotherapy for unresectable pancreatic cancer. Int J Radiat Oncol Biol Phys 2007; 68:801–8.
9. Loehrer PJ, Feng Y, Cardenes H, Wagner L, Brell JM, Cella D, et al. Gemcitabine alone versus gemcitabine plus radiotherapy in patients with locally advanced pancreatic cancer: An Eastern Cooperative Oncology Group trial. J Clin Oncol 2011;29:4105–12.
10. Huguet F, Hammel P, Vernerey D, Goldstein D, Van Laethem JL, Glimelius B, et al. Impact of chemoradiotherapy (CRT) on local control and time without treatment in patients with locally advanced pancreatic cancer (LAPC) included in the international phase III LAP 07 study. J Clin Oncol 32:5s, 2014 (suppl; abstr 4001^).
11. Koong AC, Le QT, Ho A, Fong B, Fisher G, Cho C, et al. Phase I study of stereotactic radiosurgery in patients with locally advanced pancreatic cancer. Int J Radiat Oncol Biol Phys 2004;58:1017–21.
12. Schellenberg D, Goodman KA, Lee F, Chang S, Kuo T, Ford JM, et al. Gemcitabine chemotherapy and single-fraction stereotactic body radiotherapy for locally advanced pancreatic cancer. Int J Radiat Oncol Biol Phys 2008;72:678–86.
13. Chang DT, Schellenberg D, Shen J, Kim J, Goodman KA, Fisher GA, et al. Stereotactic radiotherapy for unresectable adenocarcinoma of the pancreas. Cancer 2009;115:665–72.
14. Goodman KA, Wiegner EA, Maturen KE, Zhang Z, Mo Q, Yang G, et al. Dose-escalation study of single-fraction stereotactic body radiotherapy for liver malignancies. Int J Radiat Oncol Biol Phys 2010; 78:486–93.
15. Mahadevan A, Jain S, Goldstein M, Miksad R, Pleskow D, Sawhney M, et al. Stereotactic body radiotherapy and gemcitabine for locally advanced pancreatic cancer. Int J Radiat Oncol Biol Phys 2010;78: 735–42.
16. Herman JM, Chang DT, Goodman KA, Dholakia AS, Raman SP, Hacker-Prietz A, et al. Phase 2 multi-institutional trial evaluating gemcitabine and stereotactic body radiotherapy for patients with locally advanced unresectable pancreatic adenocarcinoma. Cancer 2015;121:1128–37.
17. Sharabi AB, Nirschl CJ, Kochel CM, Nirschl TR, Francica BJ, Velarde E, et al. Stereotactic radiation therapy augments antigen-specific PD-1-mediated antitumor immune responses via cross-presentation of tumor antigen. Cancer Immunol Res 2015;3:345–55.
18. Filatenkov A, Baker J, Mueller AMS, Kenkel J, Ahn GO, Dutt S, et al. Ablative tumor radiation can change the tumor immune cell microenvironment to induce durable complete remissions. Clin Cancer Res 2015;21:3727–39.
19. Beatty GL, Chiorean EG, Fishman MP, Saboury B, Teitelbaum UR, Sun W, et al. CD40 agonists alter tumor stroma and show efficacy against pancreatic carcinoma in mice and humans. Science 2011;331: 1612–6.
20. Lutz ER, Wu AA, Bigelow E, Sharma R, Mo G, Soares K, et al. Immunotherapy converts nonimmunogenic pancreatic tumors into immunogenic foci of immune regulation. Cancer Immunol Res 2014;2:616–31.
21. Beatty GL, Winograd R, Evans RA, Long KB, Luque SL, Lee JW, et al. Exclusion of T cells from pancreatic carcinomas in mice is regulated by $Ly6C^{low}$ $F4/80^{+}$ extratumoral macrophages. Gastroenterology 2015;149: 201–10.
22. Mantovani A, Sica A. Macrophages, innate immunity and cancer: balance, tolerance, and diversity. Curr Opin Immunol 2010;22:231–7.
23. Quail D, Joyce J. Microenvironmental regulation of tumor progression and metastasis. Nat Med 2013;19:1423–37.
24. Long KB, Gladney WL, Tooker GM, Graham K, Fraietta JA, Beatty GL. IFN-gamma and CCL2 cooperate to redirect tumor-infiltrating monocytes to degrade fibrosis and enhance chemotherapy efficacy in pancreatic carcinoma. Cancer Discov 2016;6:400–13.
25. Hingorani SR, Wang L, Multani AS, Combs C, Deramaudt TB, Hruban RH, et al. Trp53R172H and KrasG12D cooperate to promote chromosomal instability and widely metastatic pancreatic ductal adenocarcinoma in mice. Cancer Cell 2005;7:469–83.
26. Untergasser A, Cutcutache I, Koressaar T, Ye J, Faircloth BC, Remm M, et al. Primer3—new capabilities and interfaces. Nucleic Acids Res 2012;40:e115.
27. Koressaar T, Remm M. Enhancements and modifications of primer design program Primer3. Bioinformatics 2007;23:1289–91.
28. Lee Y, Auh SL, Wang Y, Burnette B, Wang Y, Meng Y, et al. Therapeutic effects of ablative radiation on local tumor require CD8+ T cells: changing strategies for cancer treatment. Blood 2009;114:589–95.
29. Clark CE, Hingorani SR, Mick R, Combs C, Tuveson DA, Vonderheide RH. Dynamics of the immune reaction to pancreatic cancer from inception to invasion. Cancer Res 2007;67:9518–27.
30. Sanford DE, Belt BA, Panni RZ, Mayer A, Deshpande AD, Carpenter D, et al. Inflammatory monocyte mobilization decreases patient survival in pancreatic cancer: a role for targeting the CCL2/CCR2 axis. Clin Cancer Res 2013;19:3404–15.
31. Serbina NV, Pamer EG. Monocyte emigration from bone marrow during bacterial infection requires signals mediated by chemokine receptor CCR2. Nat Immunol 2006;7:311–7.
32. Qian B-Z, Li J, Zhang H, Kitamura T, Zhang J, Campion LR, et al. CCL2 recruits inflammatory monocytes to facilitate breast-tumour metastasis. Nature 2011;475:222–5.
33. Li X, Yao W, Yuan Y, Chen P, Li B, Li J, et al. Targeting of tumour-infiltrating macrophages via CCL2/CCR2 signalling as a therapeutic strategy against hepatocellular carcinoma. Gut 2015 Oct 9. [Epub ahead of print].
34. Schwartz DL, Bankson JA, Lemos R, Lai SY, Arun K, He Y, et al. Radiosensitization and stromal imaging response correlates for the HIF-1 inhibitor PX-478 given with or without chemotherapy in pancreatic cancer. Mol Cancer Ther 2011;9:2057–67.
35. Mantoni TS, Lunardi S, Al-Assar O, Masamune A, Brunner TB. Pancreatic stellate cells radioprotect pancreatic cancer cells through β1-integrin signaling. Cancer Res 2011;71:3453–8.
36. Meirovitz A, Hermano E, Lerner I, Zcharia E, Pisano C, Peretz T, et al. Role of heparanase in radiation-enhanced invasiveness of pancreatic carcinoma. Cancer Res 2011;71:2772–80.
37. Watson RL, Spalding AC, Zielske SP, Morgan M, Kim AC, Bommer GT, et al. GSK3β and β-catenin modulate radiation cytotoxicity in pancreatic cancer. Neoplasia 2010;12:357–65.
38. Green CE, Liu T, Montel V, Hsiao G, Lester RD, Subramaniam S, et al. Chemoattractant signaling between tumor cells and macrophages regulates cancer cell migration, metastasis and neovascularization. PLoS One 2009;4:e6713.
39. Le DT, Wang-Gillam A, Picozzi V, Greten TF, Crocenzi T, Springett G, et al. Safety and survival with GVAX pancreas prime and Listeria monocytogenes-expressing mesothelin (CRS-207) boost vaccines for metastatic pancreatic cancer. J Clin Oncol 2015;33:1325–33.
40. Crane CH, Varadhachary GR, Yordy JS, Staerkel GA, Javle MM, Safran H, et al. Phase II trial of cetuximab, gemcitabine, and oxaliplatin

followed by chemoradiation with cetuximab for locally advanced (T4) pancreatic adenocarcinoma: correlation of Smad4(Dpc4) immunostaining with pattern of disease progression. J Clin Oncol 2011; 29:3037–43.
41. Pienta KJ, Machiels JP, Schrijvers D, Alekseev B, Shkolnik M, Crabb SJ, et al. Phase 2 study of carlumab (CNTO 888), a human monoclonal antibody against CC-chemokine ligand 2 (CCL2), in metastatic castration-resistant prostate cancer. Invest New Drugs 2013;31:760–8.
42. Gilbert J, Lekstrom-Himes J, Donaldson D, Lee Y, Hu M, Xu J, et al. Effect of CC chemokine receptor 2 CCR2 blockade on serum C-reactive protein in individuals at atherosclerotic risk and with a single nucleotide polymorphism of the monocyte chemoattractant protein-1 promoter region. Am J Cardiol 2011;107:906–11.
43. de Zeeuw D, Bekker P, Henkel E, Hasslacher C, Gouni-Berthold I, Mehling H, et al. The effect of CCR2 inhibitor CCX140-B on residual albuminuria in patients with type 2 diabetes and nephropathy: a randomised trial. Lancet Diabetes Endocrinol 2015;3:687–96.
44. Nywening TM, Wang-Gillam A, Sanford DE, Belt BA, Panni RZ, Cusworth BM, et al. Targeting tumour-associated macrophages with CCR2 inhibition in combination with FOLFIRINOX in patients with borderline resectable and locally advanced pancreatic cancer: a single-centre, open-label, dose-finding, non-randomised, phase 1b trial. Lancet 2016;17:651–62.